# VORTEX INTERACTION DYNAMICS IN TRAPPED BOSE-EINSTEIN CONDENSATES

Pedro J. Torres

Universidad de Granada, 18071 Granada, Spain

R. Carretero-González[1]

Nonlinear Physics Group, Departamento de Física Aplicada I,
Universidad de Sevilla, 41012 Sevilla, Spain

S. Middelkamp and P. Schmelcher

Zentrum für Optische Quantentechnologien,
Universität Hamburg, Luruper Chaussee 149, 22761 Hamburg, Germany

D.J. Frantzeskakis

Department of Physics, University of Athens,
Panepistimiopolis, Zografos, Athens 157 84, Greece

P.G. Kevrekidis

Department of Mathematics and Statistics,
University of Massachusetts, Amherst MA 01003-4515, USA

(Communicated by the associate editor name)

Abstract. Motivated by recent experiments studying the dynamics of configurations bearing a small number of vortices in atomic Bose-Einstein condensates (BECs), we illustrate that such systems can be accurately described by ordinary differential equations (ODEs) incorporating the precession and interaction dynamics of vortices in harmonic traps. This dynamics is tackled in detail at the ODE level, both for the simpler case of equal charge vortices, and for the more complicated (yet also experimentally relevant) case of opposite charge vortices. In the former case, we identify the dynamics as being chiefly quasi-periodic (although potentially periodic), while in the latter, irregular dynamics may ensue when suitable external drive of the BEC cloud is also considered. Our analytical findings are corroborated by numerical computations of the reduced ODE system.

1. **Introduction.** The study of vortices is a ubiquitous theme of exploration within nonlinear mathematics and physics [1]. Such topological coherent structures arise in a wide array of physical contexts ranging from fluid mechanics [2] to nonlinear optics [3, 4, 5] and the physics of superfluids, including Bose-Einstein condensates (BECs) [6, 7, 8, 9, 10, 11, 12, 13]. Among the above, BECs were shown to form a pristine setting where many of the exciting nonlinear dynamical features of single-

---

and multi-charge vortices, as well as of vortex crystals and vortex lattices, can be theoretically studied, as well as experimentally observed. In particular, after the first experimental observation of vortices in BECs [14], numerous fundamental experiments ensued. These included the production of few vortices [15] upon stirring the BEC [16] beyond a critical angular speed [15, 17, 18], but also the production of robust vortex lattices [19]. Furthermore, vortices were found to result from the interference of BEC fragments [20] (see also Refs. [21, 22, 23]), or to spontaneously occur due to the Kibble-Zurek mechanism [24]. It should also be noticed that, apart from single charge vortices, higher charge vortices were also studied in experiments [25, 26]. All the above important experimental achievements were accompanied by intense theoretical studies that have, by now, been summarized in a large number of reviews [8, 9, 10, 11, 12, 13].

In the present work, we will focus our attention on a topic of more recent interest, namely the dynamical evolution of few-vortex states. This is a line of research that was initiated theoretically by establishing the existence and robustness of the prototypical state of a so-called vortex dipole [27]. It was then more systematically examined for more complex states, such as vortex tripoles and quadrupoles [28, 29], while near-linear [30] and even strongly nonlinear/non-equilibrium effects [31] were also considered. Variants of this problem, involving dynamics of vortices in toroidal [32, 33] and anisotropic [34] traps, have been examined too. However, this area has acquired special interest very recently, due to a large range of experimental activities that have led to the creation of such few-vortex clusters, via a diverse array of experimental methods. The work of [35] produced one or more vortex dipoles by appropriate dragging of a defect through the condensate. On the other hand, the work of [36] was successful in producing three-vortex states of different types, through quadrupolar excitations of the BEC. It produced both 3 same-charge vortices in equilateral triangle configurations, and aligned configurations involving two vortices of one charge and one vortex of the opposite charge between them (the so-called tripole state). Lastly, the very recent work of [37] enabled, through its introduction of a minimally destructive imaging technique, the visualization of a time-sequence of vortex dipole dynamics near- and far from equilibrium. These recent experimental results have created a significant impetus for further theoretical study that will elucidate the dynamical properties of such vortex clusters. Such an effort should be conducted both at the level of partial differential equation (PDE) dynamics, in the context of the fundamental Gross-Pitaevskii mean-field model [6, 7, 8], as well as at the level of ordinary differential equations (ODEs), describing the precessions of vortices within the confining potential, and their mutual interactions. Our previous work [38] was a first step towards connecting the former and latter direction. The aim of the present work is to provide a systematic analysis of the ODE perspective (although we briefly discuss the connection of the PDE and ODE descriptions for completeness).

In what follows, we consider the dynamics of vortices at the level of ODEs, both for the case of same charge and for that of oppositely charged vortices. We find that the case of same charge (two-) vortices can be analytically tackled in a closed form, upon consideration of the relevant equations in the center of mass frame. We find that the motion of the vortices may be periodic or quasi-periodic, but is always analytically tractable. Notice that for both cases of same and oppositely charged vortices, we also consider a situation where the trap frequency (and, thus, the prefactor characterizing the precession of the vortex within the harmonic trap) is

time-dependent. In the case of opposite topological charges, the use of the center of mass frame is still relevant, however the dynamical picture is more complicated: in principle, the relevant evolution may not only be periodic or quasi-periodic but, in principle, it can also be chaotic (upon time modulation of the precession frequency). In addition, motivated by our numerical computations, as well as the work of [28, 29], we briefly consider some settings with 3 aligned vortices, or 4-vortex quadrupolar states.

Our presentation is structured as follows. In section 2, we give the general setup of the vortex cluster problem. Then, in section 3, we consider the equal charge two-vortex case. Section 4 consists of the opposite charge, two-vortex state. In turn, section 5 briefly considers the dynamics of different numbers of topological charges, while Section 6 summarizes our findings and presents our conclusions.

2. **Setup.** Throughout our analysis below, we will consider a BEC confined in a highly flat (alias "disk-shaped") trap, which supports stable vortex structures. This quasi-2D regime is achieved for small in-plane trapping frequency $\omega_r$ compared to the transverse trapping frequency $\omega_z$. Defining the ratio between these frequencies as $\Omega = \omega_r/\omega_z$, and considering sufficiently low temperatures, the macroscopic dynamics of the BEC can be well approximated by a $(2+1)$-dimensional Gross-Pitaevskii equation (GPE), expressed in the following dimensionless form [8]:

$$i\partial_t u = \left[ -\frac{1}{2}\nabla^2 + V(r) + |u|^2 - \mu \right] u. \tag{1}$$

Here, $u(x, y, t)$ is the (2D) macroscopic wave function normalized to the number of atoms $N = \int |u|^2 dx dy$ (with $|u|^2$ being the atomic density), $r^2 = x^2 + y^2$, $\nabla_r^2 = \partial_x^2 + \partial_y^2$ is the in-plane Laplacian, $\mu$ is the chemical potential (or the solution frequency), and the confining potential is given by

$$V(r) = \frac{1}{2}\Omega^2 r^2. \tag{2}$$

In the above equation, the density $|u|^2$, length, time and energy are respectively measured in units of $2\sqrt{2\pi}aa_z$, $a_z$, $\omega_z^{-1}$ and $\hbar\omega_z$, where $a$ and $a_z = \sqrt{\hbar/m\omega_z}$ denote, respectively, the $s$-wave scattering length and the transverse harmonic oscillator length ($m$ is the atomic mass) [8].

In this work we are interested in the dynamics of interacting vortices trapped in the harmonic trap $V(r)$. The vortex dynamics is driven by density and phase gradients of the background where the coherent structure is placed. In our case, there are two effects that need to be taken into account:

(i) The movement induced by the gradient of the background density provided by the harmonic trap that makes the BEC density inhomogeneous (the density profile resembles an inverted parabola in the so-called Thomas-Fermi approximation, relevant to the case of sufficiently large numbers of atoms [8]). This background gradient is responsible for the precession of vortices about the center of the harmonic trap [39, 40, 41, 42]. This effect is captured by the following ODEs, describing the effective motion of the vortex center $(x(t), y(t))$, for small displacements of the vortex from the center of the trap [38, 43]:

$$\dot{x} = -\omega_{\mathrm{pr}}\,S\,y, \tag{3}$$
$$\dot{y} = +\omega_{\mathrm{pr}}\,S\,x, \tag{4}$$

where $S$ denotes the vorticity (alias topological charge) of the vortex and $\omega_{\mathrm{pr}}$ its precessional frequency. In a harmonic trap with frequency $\Omega$ the precessional frequency can be well approximated by [38]

$$\omega_{\mathrm{pr}} = \frac{\Omega^2}{2\mu} \log\left(\Lambda \frac{\mu}{\Omega}\right), \tag{5}$$

where $\Lambda$ is a numerical factor taking the (approximate) value $\Lambda \approx 8.88 \approx 2\sqrt{2}\pi$ for a vortex located infinitesimally close to the origin (as the vortex departs from the origin the value of $\Lambda$ accordingly increases [38]).

(ii) The presence of another vortex induces changes in the background (density and phase) that, in turn, will induce dynamics of the vortex under consideration. Based on the analogy with fluid vortices [2], it has been argued that BEC vortices share similar interaction laws and dynamical equations. In particular, two vortices sitting on a constant background and placed sufficiently far away from each other (i.e., a few times the width of their core) at positions $(x_m, y_m)$ and $(x_n, y_n)$, interact through the effective dynamical equations [10, 11, 43]:

$$\dot{x}_m = -\, b\, S_n \frac{y_m - y_n}{r_{mn}^2}, \tag{6}$$

$$\dot{y}_m = +\, b\, S_n \frac{x_m - x_n}{r_{mn}^2}, \tag{7}$$

where $r_{mn} = \sqrt{(x_m - x_n)^2 + (y_m - y_n)^2}$ is the vortex separation, $(S_m, S_n)$ their respective vorticities such that $|S_m| = |S_n|$ (i.e., they have the same charge strength but might have opposite sign) and $b$ is a numerical factor that varies with $S \equiv |S_m| = |S_n|$; in the case of unit charge vortices ($S = 1$), the value of $b \approx 0.975$ was found to yield good agreement with results obtained in the framework of the GP Eq. (1) [38]. For all numerical results presented throughout this work we will consider, for simplicity of exposition, that $b = 1$. The net effect of this vortex-vortex interaction is that two vortices of the same charge will rotate around each other, with a constant angular velocity depending on their separation, while two oppositely charged vortices will travel parallel to each other, with a constant linear velocity depending on their separation.

Combining now both effects, namely vortex precession (induced by the harmonic trap) and vortex-vortex interactions, the effective dynamics of a small cluster of interacting vortices (of potentially different charges) can be described by the following system of ODEs:

$$\dot{x}_i = -c(t)\, S_i y_i - b \sum_{k \neq i} S_k \frac{y_i - y_k}{r_{ik}^\alpha}, \tag{8}$$

$$\dot{y}_i = +c(t)\, S_i x_i + b \sum_{k \neq i} S_k \frac{x_i - x_k}{r_{ik}^\alpha}, \qquad i = 1 \ldots n, \tag{9}$$

where $(x_i, y_i)$ and $S_i$ are, respectively, the coordinates and charge of vortex $i$, $r_{ik} = \sqrt{(x_i - x_k)^2 + (y_i - y_k)^2}$ the separation between vortex $i$ and vortex $k$, $\alpha$ and $b$ are two positive numerical constants, and the trap coefficient $c(t)$ is positive and may vary with time (see below). In this work, we leave $\alpha$ as a parameter since it does not affect the results that will be presented below. Furthermore, this, in

principle, enables the consideration of more general interaction laws other than the vortex-vortex one (which is the main motivation herein) as a function of the mutual separation of the interacting "particles". We will also allow the trap precession frequency $c(t)$ to be time dependent. In the case of a static background cloud the precession close to the background center is given by Eqs. (3)-(4) as $c(t) = \omega_{\mathrm{pr}} = (\Omega^2/(2\mu)) \log(\Lambda\mu/\Omega)$. However, as it is well known, the introduction of vortices in the BEC cloud inevitably induces dipolar (as well as higher order) excitations of the background atomic cloud. These excitations may be incorporated within the effective particle model as small periodic variations of the trap coefficient (or precession rate). Therefore, we consider the general scenario of a time-varying trap coefficient that is periodic in time with minimal period $T = 2\pi/\omega$. Since one can rescale time, let us consider, for the sake of definitiveness, a trap coefficient that in the absence of excitations of the BEC is normalized to unity, and incorporates a periodic perturbation that takes into account possible excitations of the cloud; in other words, we consider that

$$c(t) = 1 + \epsilon \sin(\omega t), \tag{10}$$

where $\epsilon$ and $\omega$ denote, respectively, the (small) amplitude and the frequency of the trap perturbation induced by the excitations of the atomic cloud. An example on how the presence of a vortex alters the properties of the underlying BEC cloud is depicted in Fig. 1. The figure shows how the width of the cloud varies periodically in time due to the presence of the precessing vortex. This produces an effective trapping constant that is perturbed periodically in time, that, in turn, induces a periodic perturbation on the precession frequency[2].

In the case of two vortices (which is the main focus of this work), the equations of motion reduce to

$$
\begin{aligned}
\dot{x}_1 &= -c(t)\, S_1\, y_1 - b\, S_2 \frac{y_1 - y_2}{r^\alpha}, \\
\dot{y}_1 &= +c(t)\, S_1\, x_1 + b\, S_2 \frac{x_1 - x_2}{r^\alpha}, \\
\dot{x}_2 &= -c(t)\, S_2\, y_2 - b\, S_1 \frac{y_2 - y_1}{r^\alpha}, \\
\dot{y}_2 &= +c(t)\, S_2\, x_2 + b\, S_1 \frac{x_2 - x_1}{r^\alpha},
\end{aligned}
\tag{11}
$$

where, for simplicity, $r \equiv r_{12}$ is the distance between the two vortices and $|S_{1,2}| = S$. An example of the comparison between the results obtained in the framework of the PDE model (1) and those obtained by this system of reduced ODEs in shown in Fig. 2. The results presented in this figure use a *constant* trap coefficient determined by the trap strength and, in turn, related to the cloud's width *before* the vortices are seeded. As it is clear from the figure, there is a very good qualitative match between the original PDE dynamics and the reduced ODEs. A number of factors are responsible for the absence of a detailed quantitative match between the two: (a) the seeding of the vortices in the BEC cloud induces oscillations of the width

---

[2]We should note in passing that experimental protocols may render important the consideration of alternative functional forms of $c(t)$ as well; in particular, in the work of [37], a minimally destructive imaging technique was introduced that periodically eliminated a small atomic fraction from the condensate in order to image it. A byproduct of this is the reduction of the atomic density and hence of the chemical potential which should lead to an increase of the precession frequency. Hence, non-oscillatory variations of $c(t)$ may be relevant to consider, although we will not pursue this aspect in further detail herein.
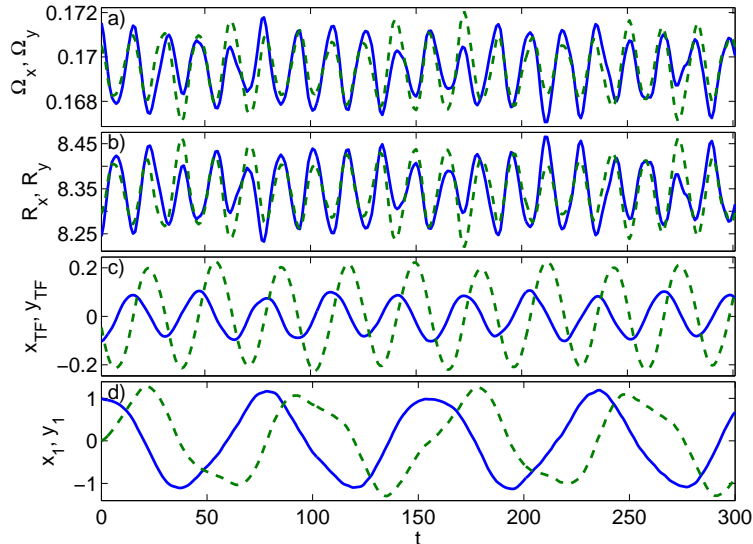
FIGURE 1. (Color online) Variations of the BEC cloud in the presence of a precessing vortex of charge $S = 1$ initially placed at $(x_1(0), y_1(0)) = (1, 0)$, as they result from the full numerical integration of Eq. (1). The corresponding value in the $x$- and $y$-direction is plotted with solid (blue) and dashed (green) lines, respectively for all panels. At each time the cloud was fitted to a Thomas-Fermi profile $u_{\mathrm{TF}}^2(x, y) = \mu - \frac{1}{2}\left(\Omega_x^2(x - x_{\mathrm{TF}})^2 + \Omega_y^2(y - y_{\mathrm{TF}})^2)\right)$ by least-square fitting the parameters $(\Omega_x, \Omega_y, x_{\mathrm{TF}}, y_{\mathrm{TF}})$. (a) Time series of the effective trapping strengths $(\Omega_x, \Omega_y)$. (b) Time series of the $x$ and $y$ Thomas-Fermi radii (i.e., width of the BEC cloud) defined by $R_i = \sqrt{2\mu}/\Omega_i$. (c) The corresponding center of the BEC cloud $(x_{\mathrm{TF}}, y_{\mathrm{TF}})$. (d) The position of the vortex as it precesses around the BEC cloud. The trap strength is $\Omega = 0.2$ and the chemical potential $\mu = 1$. The period of oscillation of the BEC cloud width corresponds to a measured breathing mode with a frequency $2\Omega$ while the cloud center oscillates with frequency $\Omega$. The measured frequency of the precessing vortex is $\omega_{\mathrm{pr}} = 0.0801$ while its estimation from Eq. (5) is $\omega_{\mathrm{pr}} = 0.0759$. The estimation is slightly lower that the measured value due to the fact that the value for the parameter $\Lambda = 8.88$ in Eq. (5) is valid for a vortex located in the immediate vicinity of the trap center, while here the vortex is macroscopically displaced from the center.

and center of the BEC cloud (cf. Fig. 1) that, in turn, change the effective trap coefficient $c(t)$; and (b) the value of the parameter $\Lambda$ in Eq. (5) should be adjusted (increased) for vortices that are not infinitesimally close to the trap's center [38].

3. **The case $S_1 = S_2$.** In this section we will study the case of $S_1 = S_2 = S$, namely the dynamics of two equal charge vortices. In fact, with a simple time rescaling we
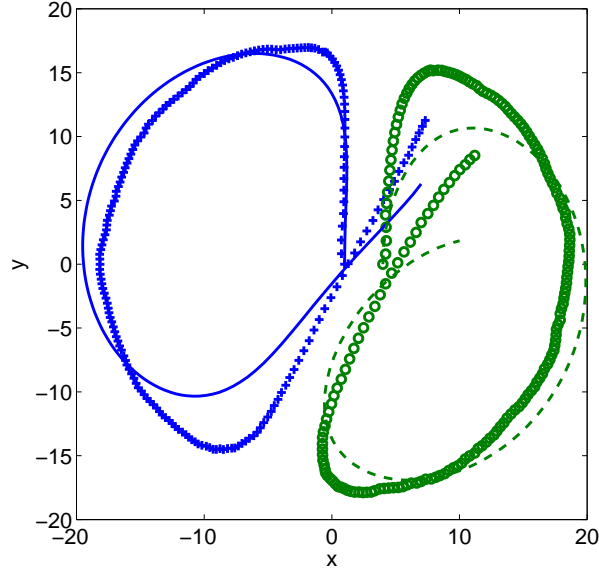
FIGURE 2. (Color online) Trajectories for two vortices of charges $S_1 = 1$ and $S_2 = -1$ in a BEC with chemical potential $\mu = 1$ trapped inside a harmonic trap of strength $\Omega = 0.05$. The vortices are initially placed at $(x_1(0), y_1(0)) = (1, 0)$ and $(x_2(0), y_2(0)) = (4, 0)$. The trajectories corresponding to the full PDE (1) are depicted by the (blue) crosses and (green) circles while the trajectories corresponding to the reduced ODE system (11) are depicted by the (blue) solid line and (green) dashed line, respectively.

can consider, without loss of generality, $S = S_1 = S_2 = 1$. Then, the system reads

$$
\begin{aligned}
\dot{x}_1 &= -c(t)\,y_1 - b\frac{y_1 - y_2}{r^\alpha}, \\
\dot{y}_1 &= +c(t)\,x_1 + b\frac{x_1 - x_2}{r^\alpha}, \\
\dot{x}_2 &= -c(t)\,y_2 - b\frac{y_2 - y_1}{r^\alpha}, \\
\dot{y}_2 &= +c(t)\,x_2 + b\frac{x_2 - x_1}{r^\alpha}.
\end{aligned}
\tag{12}
$$

We will seek the general solution of this system (which is, generally, a hopeless task for most nonlinear systems). As a first step, upon considering the new variables,

$$
s_1 = x_1 + x_2, \quad s_2 = y_1 + y_2, \quad d_1 = x_1 - x_2, \quad d_2 = y_1 - y_2, \tag{13}
$$

we can readily obtain the following equations for $s_1$ and $s_2$:

$$
\begin{aligned}
\dot{s}_1 &= -c(t)\,s_2, \\
\dot{s}_2 &= +c(t)\,s_1.
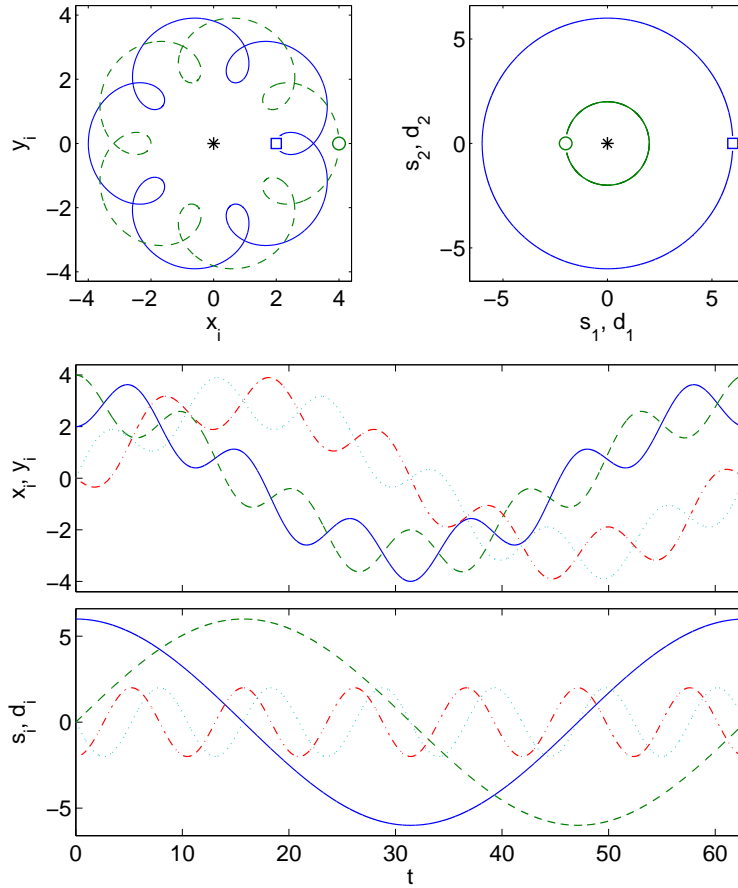\end{aligned}
\tag{14}
$$

FIGURE 3. (Color online) Periodic orbit, from the reduced ODE system (12), corresponding to two vortices of charges $S_1 = 1$ (see solid [blue] line) and $S_2 = 1$ (see dashed [green] line) with *constant* trapping coefficient $c(t) = 0.1$, vortex-vortex interaction coefficient $b = 1$ and $\alpha = 2$. The vortices are initially placed at $(x_1(0), y_1(0)) = (2, 0)$ (see [blue] square) and $(x_2(0), y_2(0)) = (4, 0)$ (see [green] circle). The top left panel depicts the actual orbit in $(x_i, y_i)$ coordinates, while the top right panel depicts the orbits in the transformed variables $(s_1, s_2)$ (see outer [blue] circle) and $(d_1, d_2)$ (see inner [green] circle). The middle and bottom panels depict the time series of the original and rescaled variables, respectively. Note that for clarity of exposition the orbit is only shown for half of its period, namely, when the first (second) vortex reaches the initial condition of the second (first) vortex.

By direct inspection, such a linear system has the general solution

$$
\begin{aligned}
s_1 &= A \cos[C(t) + B], \\
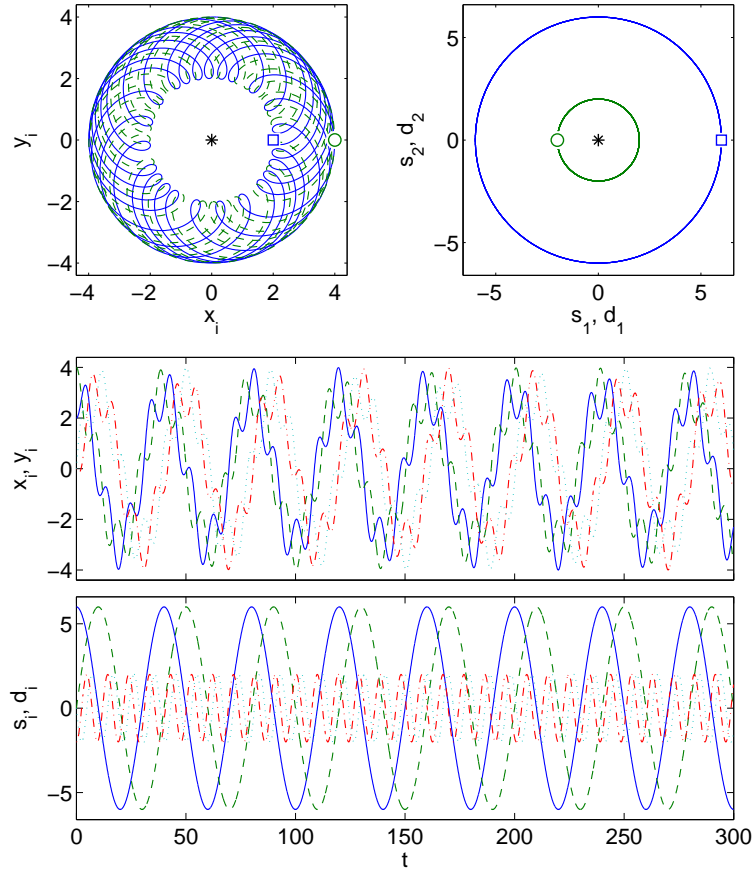s_2 &= A \sin[C(t) + B],
\end{aligned}
\tag{15}
$$

FIGURE 4. (Color online) Same as in Fig. 3 but for a quasi-periodic orbit for a constant trapping coefficient $c(t) = \pi/20$.

where $C(t) = \int_0^t c(s)ds$ and $A, B \in \mathbb{R}$. This way, we have reduced the problem to two dimensions. For $d_1$ and $d_2$, the equations of motion read

$$
\begin{aligned}
\dot{d}_1 &= -c(t)\, d_2 - \frac{2bd_2}{\left(d_1^2 + d_2^2\right)^{\alpha/2}}, \\
\dot{d}_2 &= +c(t)\, d_1 + \frac{2bd_1}{\left(d_1^2 + d_2^2\right)^{\alpha/2}}.
\end{aligned}
\tag{16}
$$

Here, we introduce polar coordinates:

$$
d_1 = r\cos\varphi, \quad d_2 = r\sin\varphi,
$$

with $r$ being the same as in Eq. (11). Now, utilizing the equation $r^2 = d_1^2 + d_2^2$, we can easily prove that

$$
r\dot{r} = d_1\dot{d}_1 + d_2\dot{d}_2 = 0,
$$

that is the radial component of system (16) is constant. In other words, $r$ is a constant of motion for our original system. For the angular variable, using $\varphi =$
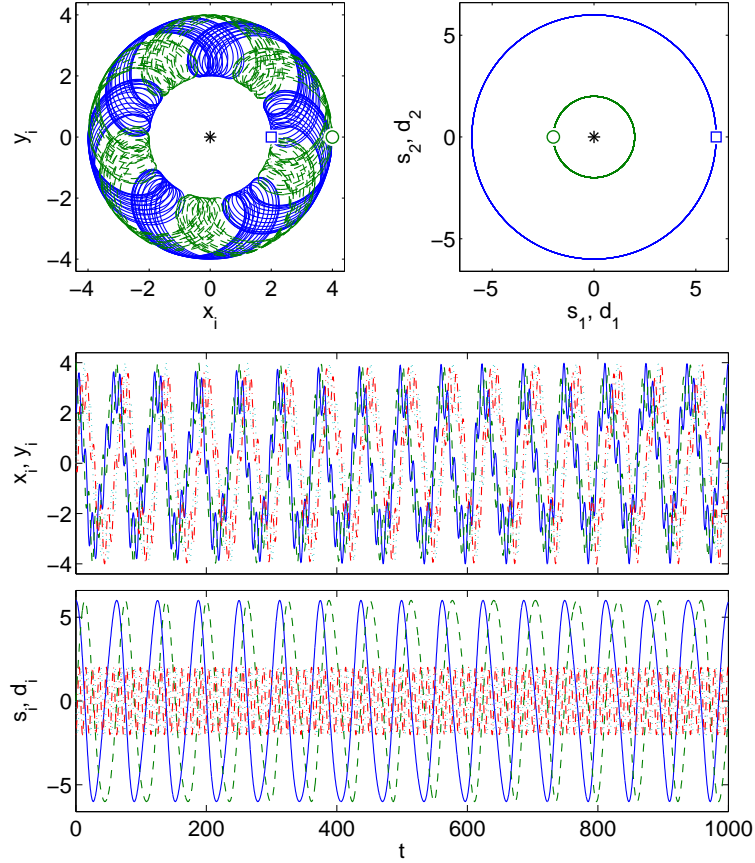
FIGURE 5. (Color online) Same as in Fig. 3 but for a quasi-periodic orbit for $c(t) = 0.1(1 + \epsilon \sin(\omega t))$ and $b = 1$ with $\epsilon = 0.25$ and $\omega = \pi/30$.

$\arctan(d_2/d_1)$ yields

$$\dot{\varphi} = \frac{d_1 \dot{d}_2 - d_2 \dot{d}_1}{r^2} = \frac{2b}{r^{\alpha/2}} + c(t).$$

Since $r$ is constant, the above equation can readily be integrated leading to the result

$$\varphi(t) = \frac{2b}{r^{\alpha/2}} t + C(t) + D,$$

where $D$ is an arbitrary constant. Thus, we have integrated the system of equations of motion (16) for two vortices of equal charge. The general solution of this system reads

$$
\begin{aligned}
d_1 &= R \cos\left( \frac{2b}{R^{\alpha/2}} t + C(t) + D \right), \\
d_2 &= R \sin\left( \frac{2b}{R^{\alpha/2}} t + C(t) + D \right),
\end{aligned}
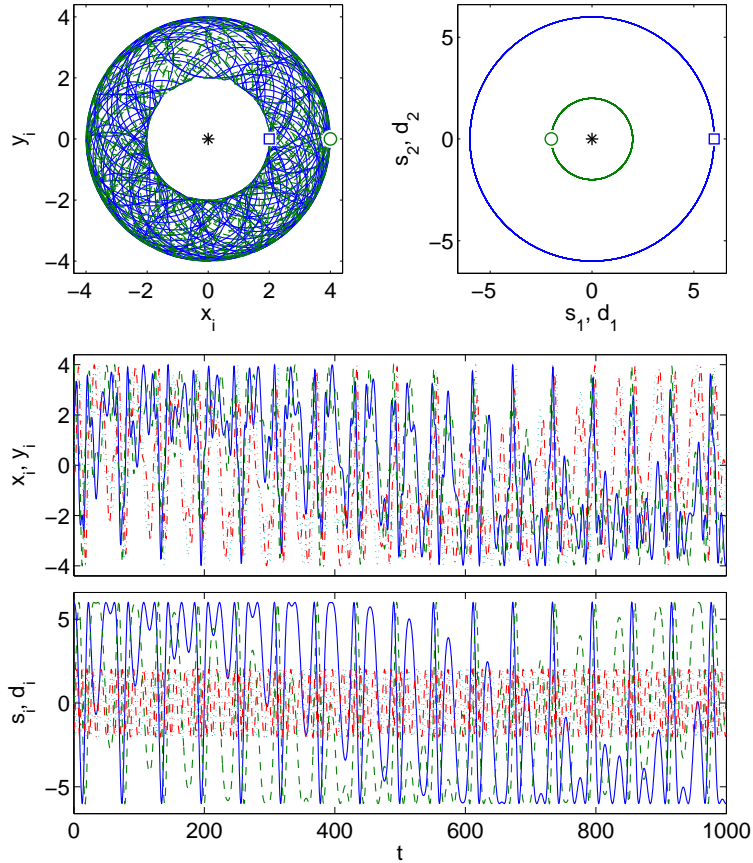\tag{17}
$$

where $D$ and $R$ are arbitrary constants.

FIGURE 6. (Color online) Same as in Fig. 5 but for a larger perturbation strength of $\epsilon = 2.5$. The apparent complex motion displayed in the top-left panel (in original coordinates) is nothing but a quasi-periodic orbit that is better elucidated in transformed coordinates in the bottom panel.

The above result shows that the solutions of the problem of the equal charge vortices, in the new coordinate system $(s_1, s_2)$ and $(d_1, d_2)$, lie in between the two circles defined by Eqs. (14) and (17). Figures 3–6 demonstrate typical examples of the corresponding orbits for different types of forcing $c(t)$. Now, it is straightforward to go back to the original variables and write the initial conditions for $(x_i, y_i)$ in terms of the arbitrary constants $A, B, R, D$. In this way, we obtain the explicit solution for the initial value problem of the system (12). Of course, everything is valid if $c$ is constant, but also for $c$ periodic or quasi-periodic. In the two first cases, generically one finds quasi-periodic solutions and there is a sequence of periodic solutions that can be obtained by fine-tuning $R$. For example, Fig. 3 depicts a periodic orbit for $c(t) = 0.1$ and $b = 1$. It is easy to observe that, since $c(t)$ and $b$ are commensurate, the resulting orbit is $40\pi$-periodic (the figure only shows half of the period). Since the dynamics for $(s_1, s_2)$ and $(d_1, d_2)$ are uncoupled, it is trivial to generate a quasi-periodic orbit by taking a constant $c(t)$ that is not

commensurate to $b$. An example of this quasi-periodic case is depicted in Fig. 4 for $c(t) = \pi/20$ and $b = 1$. Another straightforward way to obtain a quasi-periodic orbit is to introduce a time-varying $c(t) = c_0(1 + \epsilon \sin(\omega t))$ as introduced in Eq. (10) for a sufficiently small perturbation amplitude $\epsilon$ with a frequency $\omega$ that is not commensurate with $b$. An example of this quasi-periodic behavior is depicted in Fig. 5 for $c(t) = 0.1(1 + \epsilon \sin(\omega t))$ and $b = 1$ with $\epsilon = 0.25$ and $\omega = \pi/30$. Finally, if the perturbation strength $\epsilon$ is sufficiently strong, the vortices move in an apparently complex motion as depicted in Fig. 6 where the only change with respect to the previous case is a tenfold increase of $\epsilon$ (from 0.25 to 2.5). It is interesting that the apparent complex motion in the original coordinates $(x_1, y_1, x_2, y_2)$ (see top-right panel in the figure) is just a quasi-periodic motion that becomes clearer in the coordinates $(s_1, s_1, d_2, d_2)$ (see lower panel in the figure).

The case under consideration, namely that of equal charge vortices, has two constraints as it is evident from the circular orbits existing in the transformed coordinates (see top right panels in Figs. 3–6). Therefore, the dynamics of two equal charge vortices has only two effective degrees of freedom, a feature which precludes the existence of chaotic orbits (notice the differences, in this regard, to the opposite charge vortex pair considered below). Another interesting feature for all orbits of the equal charge case is that (in the original coordinates) they are *always* contained in the annulus of inner radius $R_m$ and outer radius $R_M$ where $R_m = \min\{r_1(t^*), r_2(t^*)\}$ and $R_M = \max\{r_1(t^*), r_2(t^*)\}$ where $r_1(t^*)$ and $r_2(t^*)$ are the distances of the vortices to the origin at any time $t^*$ when the vortices are aligned with the origin —a particular $t^*$ for all the numerics shown in this section is $t^* = 0$ since we always start with $y_1(0) = y_2(0) = 0$. This fact is a direct consequence of the circular shape orbits in transformed coordinates given in Eqs. (14) and (17) where $s_1^2 + s_2^2 = A^2$ and $d_1^2 + d_2^2 = R^2$.

4. **The case $S_1 = -S_2$.** In this section, we study the case of $S_1 = -S_2$, namely the dynamics of two opposite charge vortices. In fact, with a simple time rescaling, we can use $S = S_1 = -S_2 = 1$ without loss of generality. The first step in identifying the relevant vortex dynamics is a reduction to a radially symmetric Newtonian system. Let us again consider the change of variables (13). The equations of motion for $(s_1, s_2)$ and $(d_1, d_2)$ yield, respectively:

$$
\begin{aligned}
\dot{s}_1 &= +2b\frac{d_2}{r^\alpha} - c(t)\, d_2, \\
\dot{s}_2 &= -2b\frac{d_1}{r^\alpha} + c(t)\, d_1,
\end{aligned}
\tag{18}
$$

and

$$
\begin{aligned}
\dot{d}_1 &= -c(t)\, s_2, \\
\dot{d}_2 &= +c(t)\, s_1.
\end{aligned}
\tag{19}
$$

Using the change of time $\tau = C(t) \equiv \int_0^t c(s)ds$ yields the equivalent system

$$
\begin{aligned}
\dot{s}_1 &= +f(\tau)\frac{d_2}{r^\alpha} - d_2, \\
\dot{s}_2 &= -f(\tau)\frac{d_1}{r^\alpha} + d_1, \\
\dot{d}_1 &= -s_2, \\
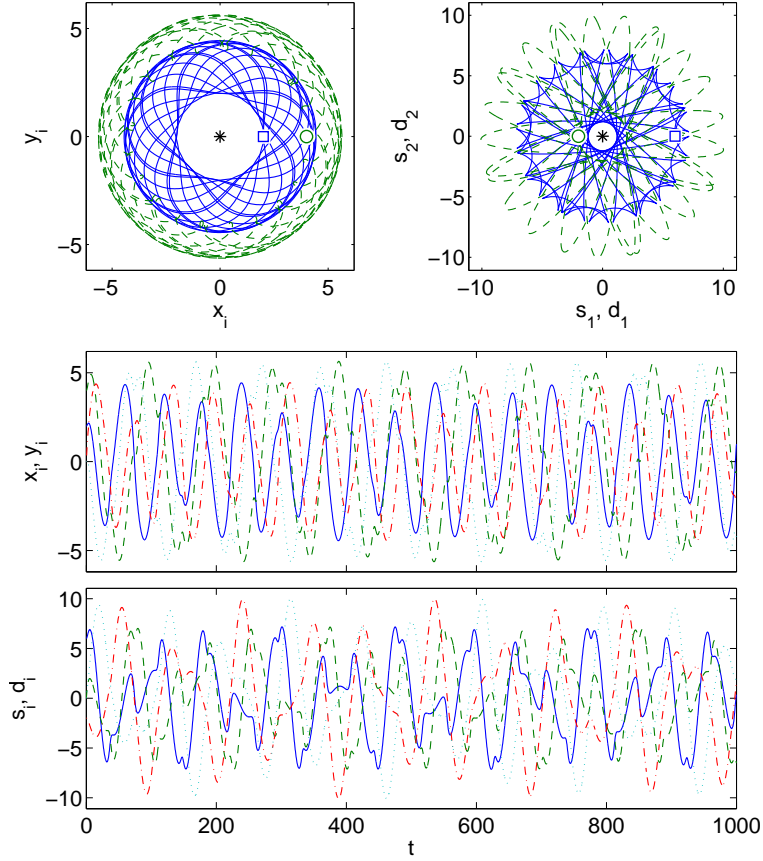\dot{d}_2 &= +s_1,
\end{aligned}
\tag{20}
$$

FIGURE 7. (Color online) Same as in Fig. 3 but for *opposite* charge vortices $S_1 = 1$ (see solid [blue] line) and $S_2 = -1$ (see dashed [green] line) with *constant* trapping coefficient $c(t) = 0.1$, vortex-vortex interaction coefficient $b = 1$ and $\alpha = 2$. The vortices are initially placed at $(x_1(0), y_1(0)) = (2, 0)$ (see [blue] square) and $(x_2(0), y_2(0)) = (4, 0)$ (see [green] circle) . The top left panel depicts the actual orbit in $(x_i, y_i)$ coordinates while the top right panel depicts the orbits in the transformed variables $(s_1, s_2)$ (see outer [blue] circle) and $(d_1, d_2)$ (see inner [green] circle). The middle and bottom panels depict the time series of the original and rescaled variables, respectively.

where $f(\tau) \equiv 2b/c(t(\tau))$. This system is periodic with the same period $(T)$ as the perturbation in Eq. (10) and it is equivalent to the following system of second order ODEs:

$$
\begin{aligned}
\ddot{d}_1 + d_1 &= f(\tau)\frac{d_1}{r^\alpha}, \\
\ddot{d}_2 + d_2 &= f(\tau)\frac{d_2}{r^\alpha}.
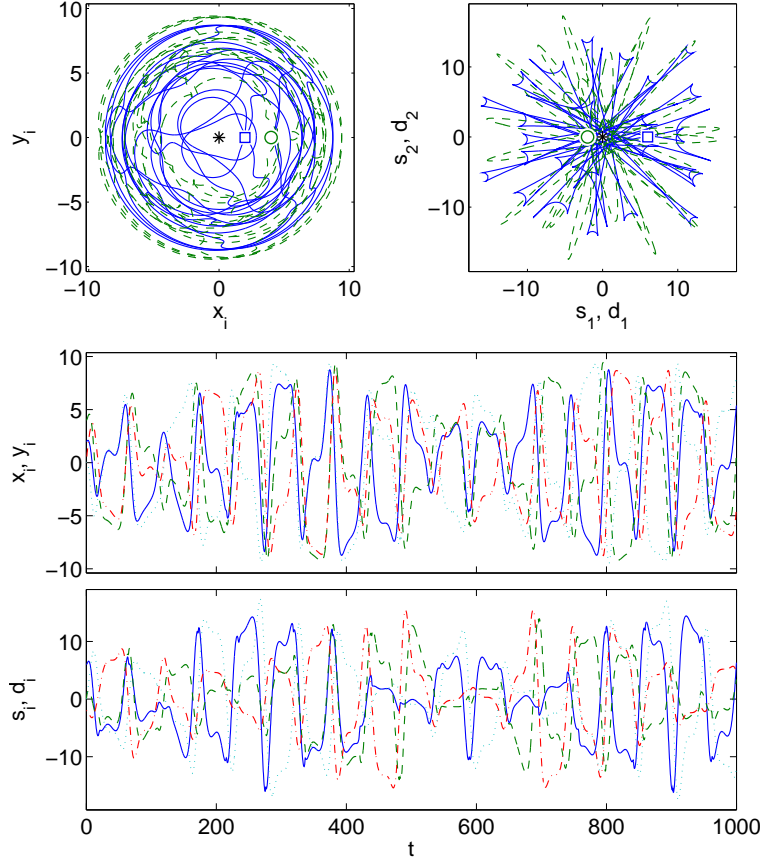\end{aligned}
\tag{21}
$$

FIGURE 8. (Color online) Same as in Fig. 7 but for an irregular orbit corresponding to $c(t) = 0.1(1 + \epsilon \sin(\omega t))$ and $b = 1$ with $\epsilon = 1$ and $\omega = 0.12$.

Recalling that $r = \sqrt{d_1^2 + d_2^2}$, one notes that this Newtonian system has a radial symmetry. This type of systems plays a central role in Celestial Mechanics and has been studied by many authors (see the review [44] and the more recent papers [45, 46, 47]).

In Figs. 7 and 8 we depict two typical scenarios for the interaction dynamics of two opposite charge vortices. Contrary to the case of equal charge vortices that has two constraints (see previous section), the case of opposite charge vortices only has a single constant of motion, the angular momentum, as described below. Therefore, the opposite charge pair allows for more complex trajectories. Figure 7 depicts a quasi-periodic orbit in the absence of periodic perturbations (i.e., $c(t) = 1$) for $b = 1$ and $\alpha = 2$. More interesting, however, is the appearance of irregular motion as one increases the perturbation strength $\epsilon$; in this case, the quasi-periodic orbit is eventually destroyed and is apparently replaced by an irregular orbit as depicted in Fig. 8. A detailed study of the chaotic properties and the parametric regions thereof falls outside of the scope of the present manuscript and will be reported in a future publication.

4.1. **Analysis of the radially symmetric system.** The main feature of a radially symmetric planar system is the conservation of angular momentum. If we consider polar coordinates

$$d_1 = r\cos(\varphi), \qquad d_2 = r\sin(\varphi),$$

the system (21) is equivalent to

$$\ddot{r} + r = \frac{\ell^2}{r^3} + \frac{f(\tau)}{r^{\alpha-1}}, \tag{22}$$

$$\dot{\varphi} = \frac{\ell}{r^2}, \tag{23}$$

where $\ell \equiv r^2 \dot{\varphi} = d_1\dot{d}_2 - d_2\dot{d}_1 = s_1d_1 + s_2d_2 = $ const. is the angular momentum of the solution $(d_1, d_2)$. Note that Eq. (22) does not depend explicitly on $\varphi$, so $\ell$ can be regarded as an independent parameter. If we find a $T$-periodic solution of Eq. (22), then the angle is given by

$$\varphi(\tau) = \int_0^\tau \frac{\ell}{r^2} ds$$

and we have that

$$r(t+T) = r(t) \qquad \varphi(t+T) = \varphi(t) + \theta,$$

where $\theta \equiv \varphi(T) = \int_0^T \ell/r^2 ds$ is the rotation number. Coming back to the Cartesian coordinates $\boldsymbol{d} = (d_1, d_2)$ and using the more convenient complex notation, we have

$$\boldsymbol{d}(t+T) = e^{i\theta}\boldsymbol{d}(t).$$

Therefore, in general we get a quasi-periodic solution of the original system. If $\theta = 0$ (stationary case) the solution $d$ is $T$-periodic, whereas if $\theta = 2\pi/k$ then $d$ is $kT$-periodic (subharmonic of order $k$).

4.2. **Constant trapping.** If $c(t)$ is a positive constant, then Eq. (22) is autonomous

$$\ddot{r} + r = \frac{\ell^2}{r^3} + \frac{2b}{cr^{\alpha-1}},$$

and, in fact, integrable. For any $\ell$, there exists a unique equilibrium $r_\ell$. Here, however, we should mention the following. Since $\ell$ is the (constant) angular momentum, $r_\ell$ gives a true equilibrium (constant solution) of the original system only if $\ell = 0$. When $\ell \neq 0$, we have an equilibrium on the amplitude or distance between vortices (this distance is constant) coupled with a rigid rotation. Such a solution is an equilibrium in the *inertial frame*; notice that it is common in Celestial Mechanics to speak about equilibria, although in fact they are rigidly rotating.

The energy function

$$V(r, \dot{r}) = \begin{cases} \dfrac{\dot{r}^2}{2} + \dfrac{r^2}{2} + \dfrac{\ell^2}{2r^2} + \dfrac{2b}{c(\alpha-2)r^{\alpha-2}} & \text{if} \quad \alpha \neq 2 \\[2mm] \dfrac{\dot{r}^2}{2} + \dfrac{r^2}{2} + \dfrac{\ell^2}{2r^2} + \dfrac{2b}{c}\ln r & \text{if} \quad \alpha = 2 \end{cases} \tag{24}$$

is constant along the orbits, therefore the orbits are the level sets of $V$, which are closed curves surrounding the equilibrium $r_\ell$. Such equilibrium is a minimum of the energy function, therefore it is stable in the Lyapunov sense. Note that this equilibrium was studied in Ref. [31]; see also Ref. [38].
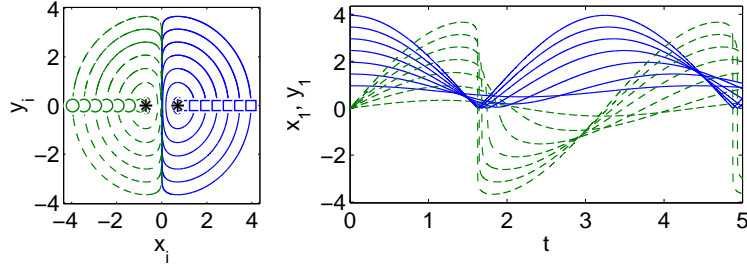
FIGURE 9. (Color online) Orbits generated around the neutrally stable stationary points (see black stars) by perturbing along the "rotating" direction (bringing vortices further apart from the center) with eigenfrequency $w_0 = \sqrt{2}$ (see text), i.e., with period $T_0 = 2\pi/\sqrt{2} \approx 4.4429$. The left panels correspond to the orbits with coordinates $(x_i, y_i)$ while the right panels corresponds to the time series for $x_1(t)$ and $y_1(t)$. The trapping and vortex-vortex coefficients are $c(t) = 1$ and $b = 1$ and $\alpha = 2$. Notice the presence of two timescales in the motion: the slow semi-circular oscillation and the fast (near-vertical) motion.

In the case $\ell = 0$, the equilibrium $r_0 = (2b/c)^{1/\alpha}$ can be explicitly computed. The associated natural (angular) frequency is $w_0 = \sqrt{\alpha}$. For the physically relevant case $\alpha = 2$, $r_\ell$ is the positive solution of the biquadratic equation

$$r^4 - \frac{2b}{c}r^2 - \ell^2 = 0.$$

The solution is

$$r_\ell = \sqrt{\frac{b}{c} + \sqrt{\frac{b^2}{c^2} + \ell^2}},$$

and the associated natural frequency is

$$w_\ell = \left[ 1 + \frac{3\ell^2}{\left( \frac{b}{c} + \sqrt{\frac{b^2}{c^2} + \ell^2} \right)^2} + \frac{2}{1 + \sqrt{1 + \frac{c^2\ell^2}{b^2}}} \right]^{1/2}.$$

In Fig. 9 we depict typical orbits close to the fixed points (black crosses). The orbits correspond to initial conditions close to the equilibrium point $r_0 = (2b/c)^{1/\alpha}$ perturbed along the eigenvector with eigenfrequency $w_0 = \sqrt{\alpha}$ that describes rotating orbits about the fixed points. The perturbation corresponds to separating the vortices out from the fixed points. It is interesting to note that the orbits emanating from these displacements are linearly (neutrally) stable and that they generate closed orbits. In consonance with the above eigenvalue study near the equilibrium points, for small displacements we can observe that the orbits have a period of $T_0 = 2\pi/\omega_0 \approx 4.4429$.

4.3. **Periodic trapping.** Here we consider the general case of $c(t) = 1 + \epsilon \sin(\omega t)$. Equation (22) belongs to a larger family of scalar second order equations studied in Ref. [48]. Using the approach therein, we can prove the following result.

**Theorem 4.1.** *Let us assume that $\omega > 2$. Then, for any $\ell \geq 0$, there exists a $T$-periodic solution of Eq. (22). Such a solution verifies the uniform bound*

$$r(t) \geq r_* := \left( \frac{2b}{1 + \epsilon} \right)^{1/\alpha} \cos\left( \frac{\pi}{\omega} \right). \tag{25}$$

**Proof.** We summarize the technique employed in Ref. [48]. First, $\omega > 2$ implies that the linear operator $Lr := \ddot{r} + r$ with $T$-periodic boundary conditions has a positive Green's function $G(t, s)$. Moreover, $G(t, s)$ can be computed explicitly. For our purposes, it is enough to point out that

$$m := \cot\left( \frac{\pi}{\omega} \right) \leq G(t, s) \leq M := 1/\sin\left( \frac{\pi}{\omega} \right)$$

and

$$\int_0^T G(t, s) ds = 1 \text{ for all } t.$$

A $T$-periodic solution of Eq. (22) is a fixed point of the operator

$$\mathcal{A}r = \int_0^T G(\tau, s) \left[ \frac{\ell^2}{r^3} + \frac{f(\tau)}{r^{\alpha-1}} \right] ds.$$

Now, it is possible to prove the existence of a fixed point of $\mathcal{A}$ by applying a well-known result for completely continuous operators in Banach spaces, due to Krasnoselskii [49]:

**Theorem 4.2.** *Let $X$ be a Banach space, and let $P \subset X$ be a cone in $X$. Assume that $\Omega_1, \Omega_2$ are open subsets of $X$ with $0 \in \Omega_1, \overline{\Omega}_1 \subset \Omega_2$ and let $\mathcal{A} : P \cap (\overline{\Omega}_2 \backslash \Omega_1) \to P$ be a completely continuous operator such that*

$$\|\mathcal{A}u\| \leqslant \|u\|, \;\; if \; u \in P \cap \partial\Omega_1$$

*and*

$$\|\mathcal{A}u\| \geqslant \|u\|, \;\; if \; u \in P \cap \partial\Omega_2.$$

*Then, $T$ has at least one fixed point in $P \cap (\overline{\Omega}_2 \backslash \Omega_1)$.*

Such a theorem can be applied to $\mathcal{A}$, by taking $X$ the Banach space of the continuous and $T$-periodic functions with the norm of the supremum, the cone

$$P = \left\{ u \in X : \min_x u \geq \frac{m}{M} \|u\| \right\},$$

and the sets

$$\Omega_1 \;\; = \;\; \left\{ u \in X : \|u\| < \left( \frac{2b}{1 + \epsilon} \right)^{1/\alpha} \right\}, \tag{26}$$

$$\Omega_2 \;\; = \;\; \left\{ u \in X : \|u\| < \frac{M}{m} R \right\}, \tag{27}$$

with $R > 0$ large enough. Using the arguments of Ref. [48], all the requirements of Theorem 4.2 can be verified (we omit further technical details for the sake of brevity). Hence, there exists a $T$-periodic solution $r \in P \cap (\overline{\Omega}_2 \backslash \Omega_1)$. This implies that for all $t$

$$r(t) \geq \frac{m}{M} \left( \frac{2b}{1 + \epsilon} \right)^{1/\alpha} = r_*,$$

so that Eq. (25) holds. $\qquad\qquad\qquad\qquad\qquad\qquad\qquad\qquad\qquad\qquad\quad \square$

The previous result gives a continuous branch of $T$-periodic solutions $(\ell, r_\ell)$ of Eq. (22). Now we analyze the stability of such solutions.

**Proposition 1.** *Take $\ell \geq 0$. Then, there exists an explicitly computable $\omega_\ell$ such that if $\omega > \omega_\ell$ then $r_\ell$ is linearly stable as a $T$-periodic solution of Eq. (22).*

**Proof.** For a Hill's equation $\ddot{y} + a(t)y = 0$, with $a(t)$ being a $T$-periodic function, there exists a wide variety of stability criteria [50, 51]. Perhaps the simplest one states that if $0 < a(t) < (\pi/T)^2$, then the Hill's equation is elliptic (that is, the Floquet multipliers are complex conjugates with norm one and not real). In our case, the linearized equation around $r_\ell$ is $\ddot{y} + a(\tau)y = 0$ with

$$a(\tau) = 1 + \frac{3\ell^2}{r_\ell^4} + \frac{(\alpha - 1)f(\tau)}{r_\ell^\alpha}.$$

Now, using the bound (25) yields

$$0 < a(\tau) \leq 1 + \frac{3\ell^2}{r_*^4} + \frac{(\alpha - 1)f(\tau)}{r_*^\alpha} = 1 + \frac{3\ell^2}{\cos^4\left(\frac{\pi}{\omega}\right)}\left(\frac{1 + \epsilon}{2b}\right)^{4/\alpha} + \frac{(1 + \epsilon)(\alpha - 1)}{(1 - \epsilon)\cos^\alpha\left(\frac{\pi}{\omega}\right)}.$$

The right-hand side is decreasing when $\omega$ tends to $+\infty$, therefore there exists $\omega_\ell > 0$ such that

$$a(\tau) < \left(\frac{\pi}{T}\right)^2 = \frac{\omega^2}{4},$$

for all $\omega > \omega_\ell$, and such $\omega_\ell$ can be computed numerically.                    $\square$

Note that we are working in a Hamiltonian framework, therefore the stability in the sense of Lyapunov cannot be directly derived from the first approximation because of the possible synchronized influence of higher terms leading to resonance. After the works of Möser [52], it is well known that the stability in the nonlinear sense depends generically on the third approximation of the periodic solution. Technically, one writes the Poincaré map in the Birkhoff's normal form, then, if its first nonlinear coefficient (i.e., first Birkhoff number) is nonzero, the solution is said to be of the twist type, and it is stable in the sense of Lyapunov.

From the point of view of KAM theory [53, 52, 54], the nonlinear terms of the Taylor's expansion around a given periodic solution are taken into account to decide the kind of dynamics arising around such a solution. The basic idea is to express the system in suitable geometrical coordinates as a perturbation of a canonical system which is integrable and, therefore, possesses invariant tori near the periodic solution. These invariant tori are persistent under perturbations and produce barriers for the flux trapping the orbits inside. As a byproduct, one obtains the typical KAM scenario around the periodic solution of twist type (see Ref. [52, 55]), including chaotic behavior derived from the existence of transversal homoclinic points for the Poincaré mapping $\mathcal{P}$, which generate Smale's horseshoe dynamics. For more details see Refs. [55, 56].

It is possible to prove analytically the presence of KAM dynamics in Eq. (22). In fact, a very similar equation was studied in Ref. [57]. For simplicity, we will consider only the case $\ell = 0$. By performing an analysis as in Ref. [57], we get the following result.

**Theorem 4.3.** *Let us assume $\ell = 0$, $\omega > \sqrt{\alpha}$, $\omega \neq \{3\sqrt{\alpha}, 4\sqrt{\alpha}\}$. Then the $T$-periodic solution $r_0$ of Eq. (22) is of twist type except possibly for a finite number of values of $\epsilon$.*

**Proof.** We only sketch the proof, since it is analogous to that of the main result in Ref. [57]. For $\epsilon = 0$, Eq. (22) reads

$$\ddot{r} + r = \frac{2b}{r^{\alpha-1}}.$$

The unique equilibrium is $r = (2b)^{1/\alpha}$, and the assumptions on the frequency $\omega$ imply that it is elliptic and out of resonances up to fourth order. Then the twist coefficient can be explicitly computed as in Sec. 4 of Ref. [57], obtaining that it is different from zero. In Proposition 1 of Ref. [57], it is proved that the twist coefficient $\beta(\epsilon)$ is an analytic function of $\epsilon$ up to multiplication by an adequate polynomial. Since an analytic function in a compact interval can vanish only in a finite number of points, the proof is complete. $\square$

4.4. **Vortex-Antivortex dynamics.** In this subsection we reinterpret the above results in our original vortex dynamical system.

**Theorem 4.4.** *Let us assume $S_1 = -S_2 = 1$ and $\omega > 2$. Then, system (11) has a continuum of quasi-periodic solutions. Moreover, there exists a $T$-periodic solution and a $NT$-periodic solution for every $N \geq N_0$.*

**Proof.** In Section 4 we proved the existence of a continuous branch $(\ell, r_\ell)$ solving Eq. (22). By defining

$$\varphi_\ell(\tau) = \int_0^\tau \frac{\ell}{r_\ell^2} ds$$

we have that

$$r_\ell(t + T) = r_\ell(t) \qquad \varphi_\ell(t + T) = \varphi_\ell(t) + \theta_\ell,$$

where $\theta_\ell = \int_0^T \ell/r_\ell^2 ds$ is the rotation number. Coming back to the original variables, we obtain a continuous branch of quasi-periodic solutions.

When $\ell = 0$, the rotation number is $\theta_0 = 0$ and we obtain a $T$-periodic solution. On the other hand, the quasi-periodic solution will be in fact $NT$-periodic when $\theta_\ell = T/N$. So the problem is to analyze the range of the function $\ell \to \theta_\ell$. Since it is continuous, its range is an interval. Note that the estimate (25) does not depend on $\ell$, therefore for every $\ell$,

$$\theta_\ell \leq \int_0^\tau \frac{\ell}{r_*^2} ds \leq \frac{\ell T}{r_*^2}.$$

This means that $\lim_{\ell \to 0^+} \theta_\ell = 0$. Therefore, there exists $N_0 > 0$ such that $\theta_\ell = T/N$ for some $\ell$ when $N > N_0$. This finishes the proof. $\square$

Concerning the stability results, it should be observed that the presented findings persist on the original system (11) only inside the manifold of constant angular momentum. If the perturbation of the solution changes the angular momentum, typical effects of higher dimensionality like Arnold diffusion may take place. On the other hand, we have illustrated the presence of irregular dynamics on system (11), although we cannot estimate quantitatively the size of such regions. However, this analytic prediction has also been corroborated by our numerical results.

We finish with a different property that may be interesting.

**Proposition 2.** *For any initial conditions of the vortices, there exists $E$ such that*

$$x_1^2 + y_1^2 = x_2^2 + y_2^2 + E.$$

*That is, the vortices' distance from the origin differs by a constant.*

**Proof.** It can be easily verified that $d_1 s_1 + d_2 s_2$ is a constant of motion, that is, its derivative is identically zero. The proof is finished if we note that $d_1 s_1 + d_2 s_2 = x_1^2 + y_1^2 - x_2^2 - y_2^2$. □

5. **Multivortex dynamics.** In this section, we try to briefly identify periodic solutions of the system (8) with a higher number of vortices. To this effect, it is convenient to rewrite the system (8) in complex variables as

$$\mathrm{i}\, \dot{z}_i = -c(t)S_i z_i - b \sum_{k \neq i} S_k \frac{z_i - z_k}{r_{ik}^{\alpha}}, \qquad i = 1, \ldots, n. \tag{28}$$

where i is the imaginary unity and $z_i = x_i + \mathrm{i}\, y_i$. If $\|.\|$ is the Euclidean norm, $r_{ik} = \|z_i - z_k\|$.
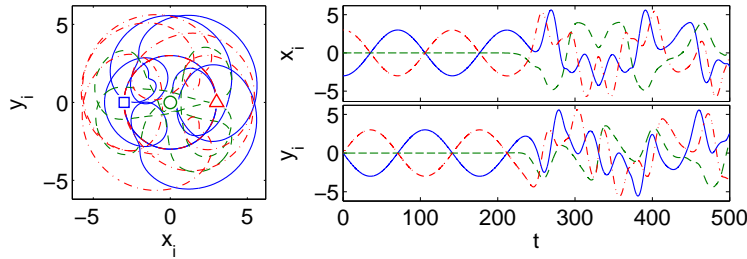


FIGURE 10. (Color online) Vortex trajectories, from the reduced ODE system (28), corresponding to three vortices of charges $S_1 = 1$ (see solid [blue] line), $S_2 = -1$ (see dashed [green] line), and $S_3 = 1$ (see dashed-dotted [red] line) with *constant* trapping coefficient $c(t) = 0.1$, vortex-vortex interaction coefficient $b = 1$ and $\alpha = 2$. The vortices are initially placed at $(x_1(0), y_1(0)) = (-3, 0)$ (see [blue] square), $(x_2(0), y_2(0)) = (0, 0)$ (see [green] circle), and $(x_3(0), y_3(0)) = (3, 0)$ (see [red] triangle). The left panel depicts the actual orbit in $(x_i, y_i)$ coordinates. The right panels depict the time series of the original $x_i$ (top) and $y_i$ (bottom) variables, respectively.

5.1. **Three vortex dynamics.** Let us begin with the case of three vortices $(n = 3)$.

**Theorem 5.1.** *Let us assume $n = 3$ and $S_1 = S_3$. Let $z$ be a solution of the equation*

$$\mathrm{i}\, \dot{z} = -c(t)S_1 z - b \left( S_2 + 2^{1-\alpha} S_1 \right) \frac{z}{\|z\|^{\alpha}}. \tag{29}$$

*Then, $z_1 = z, z_2 = 0, z_3 = -z$ is a solution of system (28).*

The proof is done by direct substitution. Interestingly, the symmetry of the solution implies that no assumption is made over $S_2$ —however, the rotation rate of the orbit does depend on the different combinations of $S_1$ and $S_2$, see below.
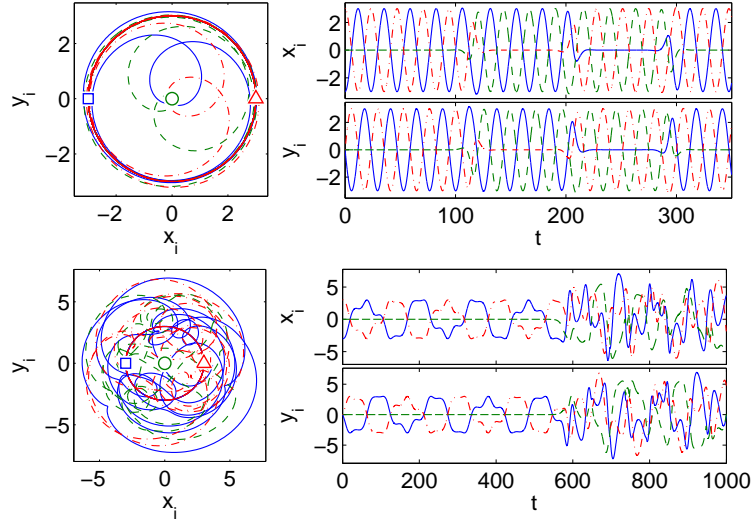
FIGURE 11. (Color online) Top set of panels: same as in Fig. 10 but for equal charges $S_1 = S_2 = S_3 = 1$. Bottom set of panels: same as in Fig. 10 but with periodic trapping $c(t) = 0.1(1 + \epsilon \sin(\omega t))$ with $\epsilon = 0.5$ and $\omega = 0.12$.
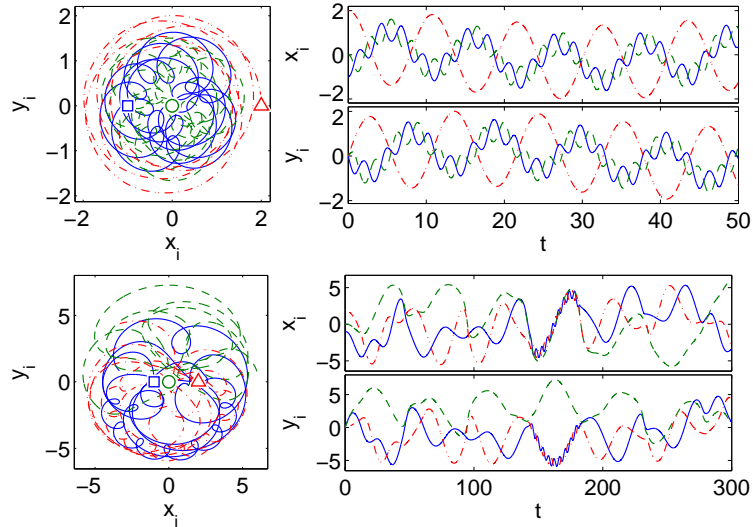


FIGURE 12. (Color online) Same as in Fig. 10 but for the for asymmetric initial positions $(x_1(0), y_1(0)) = (-1, 0)$, $(x_2(0), y_2(0)) = (0, 0)$, and $(x_3(0), y_3(0)) = (2, 0)$. Top set of panels: equal charges $S_1 = S_2 = S_3 = 1$. Bottom set of panels: same charges as in Fig. 10, i.e., $(S_1, S_2, S_3) = (+1, -1, +1)$.

By separating real and imaginary parts ($z = x + iy$), Eq. (29) is equivalent to the system

$$\begin{aligned} \dot{x} &= -c(t)S_1 y - \frac{\hat{b}y}{(x^2 + y^2)^{\alpha/2}}, \\ \dot{y} &= +c(t)S_1 x + \frac{\hat{b}x}{(x^2 + y^2)^{\alpha/2}}, \end{aligned} \tag{30}$$

where $\hat{b} = b\left(S_2 + 2^{1-\alpha}S_3\right)$. This system was integrated in Section 3, in fact it is exactly the same system as given in Eq. (16). Repeating the same arguments, the general solution is given by

$$x = R\cos\left(\frac{\hat{b}}{R^{\alpha/2}}t + C(t) + D\right), \tag{31}$$

$$y = R\sin\left(\frac{\hat{b}}{R^{\alpha/2}}t + C(t) + D\right) \tag{32}$$

where $D$ and $R$ are arbitrary constants.

An example of the orbit described in Theorem 5.1 is depicted in Fig. 10 where two equal charge vortices ($S_1 = S_3 = 1$) placed diagonally opposite from each other while the remaining vortex sits at the center with opposite charge ($S_2 = -1$). As it can be observed from the figure, the orbit starts with a solid rigid rotation (i.e., the solutions described in Theorem 5.1). However, this orbit is unstable and, after some time ($t > 250$), the motion of the vortices becomes irregular. If one chooses the central vortex to have the *same* charge as the diagonally opposite vortices the corresponding orbit (see top panels in Fig. 11 where $S_1 = S_2 = S_3 = 1$) is also unstable. However, the instability does not lead to an irregular orbit as in the previous case. In fact, as it is depicted in the top row of panels in Fig. 11, the rigid rotation is replaced by a periodic exchange of the role of the vortices where each vortex takes cyclic turns to occupy the center of the trap while the other two vortices remain in rigid rotation. These periodic windows are accompanied by a fast transitional exchange of the vortices.

Similar behavior to the unstable rigid rotation is obtained when introducing a non constant periodic trapping. For example, in the bottom panels of Fig. 11 we use the same configuration as in Fig. 10 but with a periodic trapping $c(t) = 0.1(1+\epsilon\sin(\omega t))$ with $\epsilon = 0.5$ and $\omega = 0.12$. As it can be noticed, the rigid rotation circular orbit is still preserved (as it was for the case of *two* equal charge vortices examined earlier), but in this case it is quasi-periodic. As for the constant trapping case, the rigid rotation orbit is unstable and, after some time ($t > 600$), settles to an irregular motion.

On the other hand, if one starts with an asymmetric initial condition we no longer obtain orbits with rigid rotation. However, the nature of the resulting orbits crucially depends on the relative signs of the vortex charges. For example, if one takes all the vortices with the *same* charge, in analogy to the case with two vortices studied earlier, one should expect a more regular type of behavior than when the vortices have *different* charges. This is indeed the case as it is depicted in the top row of panels in Fig. 12 where the asymmetric initial configuration of three equal charge vortices ($S_i = 1$) evolves into an apparent quasi-periodic orbit. However, if one of these vortices is imprinted with a charge that is opposite from the other two, the resulting orbit is much more complicated as it can be evidenced from the bottom row of the panels in Fig. 12. This case has the same configuration and parameters as the top row of panels but the charge of the vortex at the center has been switched ($S_3 = -1$). The resulting irregular motion has some interesting features, for example, the two vortices with the same charge tend to "meet" each other from time to time and quickly rotate around each other (due to the vortex-vortex interaction) until the other vortex disturbs them. This effect can be clearly observed in the time series for the positions of the vortices (right subpanels) where,

in the time interval $140 < t < 180$, the first (see [blue] solid line) and third (see [red] dashed-dotted line) vortices rotate around each other. We have observed that this bound pair repeats itself sporadically for longer times as well.
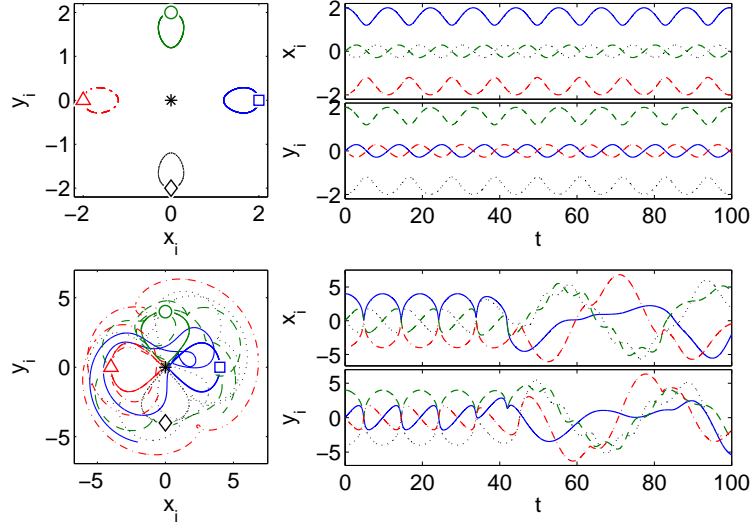


FIGURE 13. (Color online) Vortex trajectories, from the reduced ODE system (33), corresponding to four vortices of charges $S_1 = 1$ (see solid [blue] line), $S_2 = -1$ (see dashed [green] line), $S_3 = 1$ (see dashed-dotted [red] line), and $S_4 = -1$ (see dotted [black] line) with *constant* trapping coefficient $c(t) = 0.2$, vortex-vortex interaction coefficient $b = 1$ and $\alpha = 2$. The vortices are initially placed at $(x_1(0), y_1(0)) = (2, 0)$ (see [blue] square), $(x_2(0), y_2(0)) = (0, 2)$ (see [green] circle), $(x_3(0), y_3(0)) = (-2, 0)$ (see [red] triangle), and $(x_4(0), y_4(0)) = (0, -2)$ (see [black] diamond). The left panel depicts the actual orbit in $(x_i, y_i)$ coordinates. The right panels depict the time series of the original $x_i$ (top) and $y_i$ (bottom) variables, respectively. The bottom panels show the same configuration but with 2 replaced by 4 everywhere in the (symmetric) initial displacements above.

5.2. **Four vortex dynamics.** In the case of four vortices, we can perform an analogous analysis for the charge checkerboard configuration

$$
\begin{array}{cc}
+ & - \\
- & +
\end{array}
$$

**Theorem 5.2.** *Let us assume $n = 4$ and*

$$S_1 = S_3, \ S_2 = S_4, \ \text{and} \ S_1 = -S_2.$$

*Let $z$ be a solution of the equation*

$$i\,\dot{z} = -c(t)S_1 z - bS_1 \left( 2^{1-\alpha/2} - 2^{1-\alpha}S_1 \right) \frac{z}{\|z\|^\alpha}. \tag{33}$$

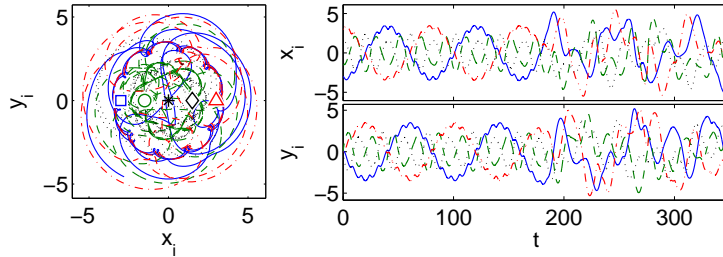*Then, $(z_1, z_2, z_3, z_4) = (z, iz, -z, -iz)$ is a solution of system (28).*

FIGURE 14. (Color online) Same as in Fig. 13 but with the vortices initially placed at $(x_1(0), y_1(0)) = (-3, 0)$ (see [blue] square), $(x_2(0), y_2(0)) = (-1.5, 0)$ (see [green] circle), $(x_3(0), y_3(0)) = (1.5, 0)$ (see [red] triangle), and $(x_4(0), y_4(0)) = (3, 0)$ (see [black] diamond).
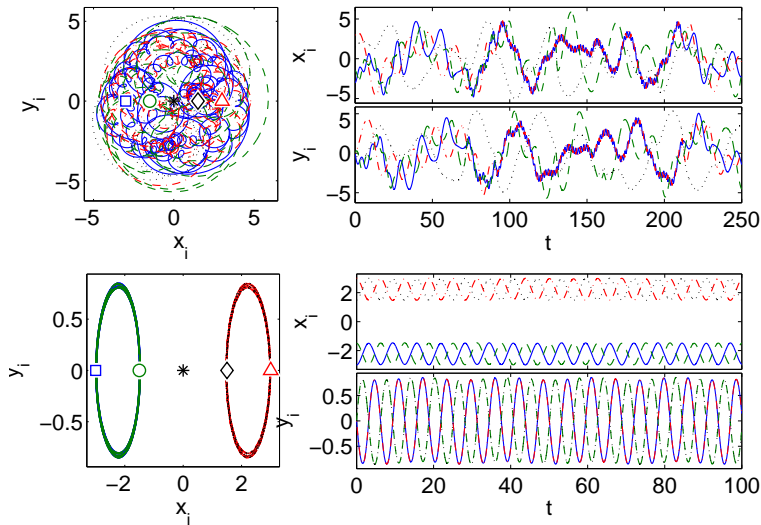


FIGURE 15. (Color online) Same as in Fig. 14 but for charges $(S_1, S_2, S_3, S_4) = (+1, +1, +1, -1)$ (top set of panels) and $(S_1, S_2, S_3, S_4) = (+1, +1, -1, -1)$ (bottom set of panels).

As before, Eq. (33) is explicitly integrable. As in the case for two equal charge vortices, this system also contains a fixed point with neutrally stable orbits around it. A more detailed study of the fixed points and the periodic orbits existing around them falls outside of the scope of the present paper. Nonetheless, in Fig. 13 we depict a pair of examples of the orbits generated near the fixed point. The top set of panels corresponds to a stable periodic orbit close to the fixed point and the bottom set of panels corresponds to an *unstable* periodic orbit when the vortices are initially located further away from the fixed point. The above results are pointers towards generalizations in the case of higher numbers of vortices, which can, in turn, possess periodic orbits upon suitable symmetric selection of the vortex locations. For example in Fig. 14 we use the same charges as in Fig. 13 but with a different

initial configuration with the four vortices aligned with alternating charges. The result is an *unstable* quasi periodic orbit that eventually settles to a chaotic orbit. If the same configuration as in Fig. 14 is used but the charges are not symmetrically placed one immediately obtains an irregular orbit as it is depicted in the top panels of Fig. 15. On the other hand, if the charges are chosen anti-symmetrically with respect to the origin, it is possible to obtain *stable* periodic and quasi-periodic orbits with bound vortex pairs of equal charge as depicted in the bottom panels of Fig. 15.

6. **Discussion and Conclusions.** It is evident that the problem of vortex interaction dynamics presents significant analogies with the classical $N$-body problem of Celestial Mechanics. For instance, we have seen that the two-vortex interaction is explicitly integrable, just as the 2-body problem. Concerning multi-vortex interaction, the collinear solution found in Subsection 5.1 resembles the straight-line solution for the 3-body problem given by Euler in 1767, whereas the four-vortex solution found in Subsection 5.2 is an analogous of the equilateral Lagrangian solution. Therefore, it is plausible to conjecture the appearance of more complicated solutions like an analogous of the Chenciner-Montgomery figure-eight solution [58] for the three-vortex case, among others.

Our aim in the present work was to explore some of the prototypical possibilities within the vortex dynamics of predominantly the two-vortex case (of both same and opposite topological charges). The same-charge case is apparently the simpler one, since its solution can be derived in closed analytical form in the center of mass frame of coordinates (even for time-dependent precession frequencies). The opposite-charge case can become more complicated and the introduction of time-dependent precession may in principle even lead to chaotic dynamics, while in the same charge case, the dynamics can be, at most, quasi-periodic.

Naturally, a systematic examination of the higher number of charge cases (some prototypical examples of which we have also considered herein illustrating their potential for fixed points, periodic or quasi-periodic motions), as well as the identification of chaotic regions of the simplest two-opposite-charge case are among the principal themes that deserve further exploration. Such studies are currently in progress and will be reported elsewhere.

## REFERENCES

[1] L.M. Pismen, "Vortices in Nonlinear Fields", Oxford Science Publications, Oxford, 1999.
[2] A.J. Chorin and J.E. Marsden, "A Mathematical Introduction to Fluid Mechanics", Springer-Verlag, New York, 1993.
[3] Yu.S. Kivshar, J. Christou, V. Tikhonenko, B. Luther-Davies, and L.M. Pismen, *Dynamics of optical vortex solitons*, Opt. Commun., **152** (1998), 198–206.
[4] A. Dreischuh, S. Chevrenkov, D. Neshev, G.G. Paulus, and H. Walther, *Generation of lattice structures of optical vortices*, J. Opt. Soc. Am. B, **19** (2002), 550–556.

[5] A.S. Desyatnikov, Yu.S. Kivshar, and L. Torner, *Optical vortices and vortex solitons*, Prog. Optics, **47** (2005), 291–391.

[6] L. P. Pitaevskii and S. Stringari, "Bose-Einstein Condensation", Oxford University Press, Oxford, 2003.

[7] C.J. Pethick and H. Smith, "Bose-Einstein condensation in dilute gases", Cambridge University Press, Cambridge, 2002.

[8] P. G. Kevrekidis, D. J. Frantzeskakis, and R. Carretero-González, "Emergent Nonlinear Phenomena in Bose-Einstein Condensates. Theory and Experiment", Springer-Verlag, Berlin, 2008.

[9] A. L. Fetter and A. A. Svidzinksy, *Vortices in a trapped dilute Bose-Einstein condensate*, J. Phys.: Cond. Matt. (2001) **13**, R135–R194.

[10] P. G. Kevrekidis, R. Carretero-González, D. J. Frantzeskakis, and I. G. Kevrekidis, *Vortices in Bose-Einstein Condensates: Some Recent Developments*, Mod. Phys. Lett. B, **18** (2004), 1481–1505.

[11] P. K. Newton and G. Chamoun, *Vortex lattice theory: A particle interaction perspective*, SIAM Rev., **51** (2009), 501–542.

[12] R. Carretero-González, P.G. Kevrekidis, and D.J. Frantzeskakis, *Nonlinear waves in Bose-Einstein condensates: physical relevance and mathematical techniques*, Nonlinearity, **21** (2008), R139–R202.

[13] A. L. Fetter, *Rotating trapped Bose-Einstein condensates*, Rev. Mod. Phys., (2009) **81**, 647–691.

[14] M.R. Matthews, B.P. Anderson, P.C. Haljan, D.S. Hall, C.E. Wieman, and E.A. Cornell, *Vortices in a Bose-Einstein Condensate*, Phys. Rev. Lett. **83** (1999), 2498–2501.

[15] K.W. Madison, F. Chevy, V. Bretin, and J. Dalibard, *Stationary States of a Rotating Bose-Einstein Condensate: Routes to Vortex Nucleation*, Phys. Rev. Lett. **86** (2001), 4443–4446.

[16] K. W. Madison, F. Chevy, W. Wohlleben, and J. Dalibard, *Vortex Formation in a Stirred Bose-Einstein Condensate*, Phys. Rev. Lett. **84** (2000), 806–809.

[17] A. Recati, F. Zambelli, and S. Stringari, *Overcritical Rotation of a Trapped Bose-Einstein Condensate* Phys. Rev. Lett. **86** (2001), 377–380.

[18] S. Sinha and Y. Castin, *Dynamic Instability of a Rotating Bose-Einstein Condensate*, Phys. Rev. Lett. **87** (2001), 190402.

[19] C. Raman, J.R. Abo-Shaeer, J.M. Vogels, K. Xu, and W. Ketterle, *Vortex Nucleation in a Stirred Bose-Einstein Condensate*, Phys. Rev. Lett. **87** (2001), 210402.

[20] D.R. Scherer, C.N. Weiler, T.W. Neely, and B.P. Anderson, *Vortex Formation by Merging of Multiple Trapped Bose-Einstein Condensates*, Phys. Rev. Lett. **98** (2007), 110402.

[21] R. Carretero-González, N. Whitaker, P.G. Kevrekidis, and D.J. Frantzeskakis, *Vortex structures formed by the interference of sliced condensates*, Phys. Rev. A, **77** (2008), 023605.

[22] R. Carretero-González, B.P. Anderson, P.G. Kevrekidis, D.J. Frantzeskakis, and C.N. Weiler, *Dynamics of vortex formation in merging Bose-Einstein condensate fragments*, Phys. Rev. A, **77** (2008), 033625.

[23] G. Ruben, D.M. Paganin, and M. J. Morgan, *Vortex-lattice formation and melting in a nonrotating Bose-Einstein condensate*, Phys. Rev. A, **78** (2008), 013631.

[24] C.N. Weiler, T.W. Neely, D.R. Scherer, A.S. Bradley, M.J. Davis, and B.P. Anderson, *Spontaneous vortices in the formation of Bose-Einstein condensates*, Nature, **455** (2008), 948–951.

[25] A.E. Leanhardt, A. Görlitz, A.P. Chikkatur, D. Kielpinski, Y. Shin, D.E. Pritchard, and W. Ketterle, *Imprinting Vortices in a Bose-Einstein Condensate using Topological Phases*, Phys. Rev. Lett., **89** (2002), 190403; Y. Shin M. Saba, M. Vengalattore, T.A. Pasquini, C. Sanner, A.E. Leanhardt, M. Prentiss, D. E. Pritchard, and W. Ketterle, *Dynamical Instability of a Doubly Quantized Vortex in a Bose-Einstein Condensate*, Phys. Rev. Lett. **93** (2004), 160406.

[26] T. Isoshima, M. Okano, H. Yasuda, K. Kasa, J. A. M. Huhtamäki, M. Kumakura, and Y. Takahashi, *Spontaneous splitting of a quadruply charged vortex*, Phys. Rev. Lett., **99** (2007), 200403.

[27] L.-C. Crasovan, V. Vekslerchik, V. M. Pérez-García, J. P. Torres, D. Mihalache, and L. Torner, *Stable vortex dipoles in nonrotating Bose-Einstein condensates*, Phys. Rev. A, **68** (2003), 063609.

[28] M. Möttönen, S.M.M. Virtanen, T. Isoshima, and M.M. Salomaa, *Stationary vortex clusters in nonrotating Bose-Einstein condensates*, Phys. Rev. A, **71** (2005), 033626.

[29] V. Pietilä, M. Möttönen, T. Isoshima, J.A.M. Huhtamäki and S.M.M. Virtanen, *Stability and dynamics of vortex clusters in nonrotated Bose-Einstein condensates*, Phys. Rev. A, **74** (2006), 023603.

[30] A. Klein, D. Jaksch, Y. Zhang, and W. Bao, *Dynamics of vortices in weakly interacting Bose-Einstein condensates*, Phys. Rev. A, **76** (2007), 043602.

[31] W. Li, M. Haque, and S. Komineas, *Vortex dipole in a trapped two-dimensional Bose-Einstein condensate*, Phys. Rev. A, **77** (2008), 053610.

[32] J.-P. Martikainen, K.-A. Suominen, L. Santos, T. Schulte, and A. Sanpera, *Generation and evolution of vortex-antivortex pairs in Bose-Einstein condensates*, Phys. Rev. A, **64** (2001), 063602.

[33] T. Schulte, L. Santos, A. Sanpera, and M. Lewenstein, *Vortex-vortex interactions in toroidally trapped Bose-Einstein condensates*, Phys. Rev. A, **66** (2002), 033602.

[34] S. McEndoo and Th. Busch, Small numbers of vortices in anisotropic traps, Phys. Rev. A, **79** (2009), 053616.

[35] T.W. Neely, E.C. Samson, A.S. Bradley, M.J. Davis, and B.P. Anderson, *Observation of Vortex Dipoles in an Oblate Bose-Einstein Condensate*, Phys. Rev. Lett., **104** (2010), 160401.

[36] J.A. Seman, E.A.L. Henn, M. Haque, R.F. Shiozaki, E.R.F. Ramos, M. Caracanhas, P. Castilho, C. Castelo Branco, K.M.F. Magalhães, and V.S. Bagnato, *Three-vortex configurations in trapped Bose-Einstein condensates*, arXiv:0907.1584.

[37] D.V. Freilich, D.M. Bianchi, A.M. Kaufman, T.K. Langin, and D.S. Hall, *Experimental Visualization of Vortex Dynamics in a Bose-Einstein Condensate*, submitted.

[38] S. Middelkamp, P. G. Kevrekidis, D. J. Frantzeskakis, R. Carretero-González, and P. Schmelcher, *Bifurcations, Stability and Dynamics of Multiple Matter-Wave Vortex States*, to appear in Phys. Rev. A, 2010.

[39] B. Jackson, J. F. McCann, and C. S. Adams, *Vortex line and ring dynamics in trapped Bose-Einstein condensates*, Phys. Rev. A, **61** (1999), 013604.

[40] A.A. Svidzinsky and A.L. Fetter, *Stability of a Vortex in a Trapped Bose-Einstein Condensate*, Phys. Rev. Lett., **84** (2000), 5919–5923.

[41] J. Tempere and J.T. Devreese, *Vortex dynamics in a parabolically confined Bose-Einstein condensate*, Solid State Comm., **113** (2000), 471–474.

[42] B.P. Anderson, P.C. Haljan, C.E. Wieman, and E.A. Cornell, *Vortex Precession in Bose-Einstein Condensates: Observations with Filled and Empty Cores*, Phys. Rev. Lett., **85** (2000), 2857–2860.

[43] S. Middelkamp, P.G. Kevrekidis, D.J. Frantzeskakis, R. Carretero-Gonz/'alez, and P. Schmelcher, J. Phys. B: At. Mo. Opt. Phys. **43** (2010) 155303.

[44] A. Ambrosetti, and V. Coti Zelati, "Periodic solutions of singular Lagrangian systems", Birkhäuser Boston, Boston, MA, 1993.

[45] A. Fonda and R. Toader, *Periodic orbits of radially symmetric Keplerian-like systems: a topological degree approach*, J. Differential Equations, **244** (2008), 3235–3264.

[46] A. Fonda and R. Toader, *Periodic orbits of radially symmetric systems with a singularity: the repulsive case*, Quaderno Matematico n. 592 (2009), Università di Trieste. Preprint available at http://www.dmi.units.it/ fonda/pubblicazioni.html.

[47] A. Fonda, A. J. Ureña, *Periodic, subharmonic, and quasi-periodic oscillations under the action of a central force*, to appear in Discrete Continuous Dynam. Systems, preprint available at http://www.ugr.es/ ecuadif/fuentenueva.htm.

[48] P.J. Torres, *Existence of one-signed periodic solutions of some second-order differential equations via a Krasnoselskii fixed point theorem*, J. Diff. Eq., **190** (2003), 643–662.

[49] M.A. Krasnoselskii, "Positive solutions of operator equations", Groningen: Noordhoff, 1964.

[50] W. Magnus and S. Winkler, "Hill's Equation", Dover, New York, 1979.

[51] V.M. Starzinskii, *Survey of works on conditions of stability of the trivial solution of a system of linear differential equations with periodic coefficients*, Amer. Math. Soc. Transl., Ser. 2, Vol.1, Providence, RI, 1955.

[52] C. L. Siegel, J. K. Moser, "Lectures on Celestial Mechanics", Springer-Verlag, New York. Berlin, 1971.

[53] V. Arnold, ”Methodes Matémathiques de la Mécanique Classique,” Mir. Moscow, 1976.

[54] J. Möser, *On invariant curves of area -preserving mappings of an annulus*, Nachr. Akad. Wiss. Göttingen Math. Phys. Kl. II (1962) 1–20.

[55] S. Newhouse, *Quasi-Elliptic Periodic Points in Conservative Dynamical Systems*, American Journal of Mathematics, **99**, N-+5, (1977) 1061–1087.

[56] C. Genecand, *Transversal homoclinic orbits near elliptic fixed points of area-preserving diffeomorphisms of the plane*, in "Dynam. Report. Expositions Dynam. Systems" (N.S.), 2, Springer, Berlin, 1993.

[57] P.J. Torres, *Twist solutions of a Hill's equation with singular term*, Adv. Nonlinear Stud., **2** (2002), 279–287.

[58] A. Chenciner, R. Montgomery, *A Remarkable Periodic Solution of the Three-Body Problem in the Case of Equal Masses*, Ann. Math., **152** (2000) 881–901.

*E-mail address*: `ptorres@ugr.es`

*E-mail address*: `carreter@sciences.sdsu.edu`

*E-mail address*: `smiddelk@physnet.uni-hamburg.de`

*E-mail address*: `pschmelc@physnet.uni-hamburg.de`

*E-mail address*: `dfrantz@phys.uoa.gr`

*E-mail address*: `kevrekid@gmail.com`